JACS
JOURNAL OF THE AMERICAN CHEMICAL SOCIETY
Article
pubs.acs.org/JACS

Engineered Asymmetric Heterogeneous Membrane: A Concentration-Gradient-Driven Energy Harvesting Device

Zhen Zhang,[†] Xiang-Yu Kong,[‡] Kai Xiao,[†] Qian Liu,[§] Ganhua Xie,[†] Pei Li,[†] Jie Ma,[‡] Ye Tian,[†] Liping Wen,[*,‡] and Lei Jiang[†,‡]

[†]Beijing National Laboratory for Molecular Sciences (BNLMS), Key Laboratory of Organic Solids, Institute of Chemistry, Chinese Academy of Sciences, Beijing 100190, P. R. China

[‡]Laboratory of Bioinspired Smart Interfacial Science, Technical Institute of Physics and Chemistry, Chinese Academy of Sciences, Beijing 100190, P. R. China

[§]Beijing Key Laboratory of Energy Conversion and Storage Materials, College of Chemistry, Key Laboratory of Theoretical and Computational Photochemistry, Ministry of Education, Beijing Normal University, Beijing 100875, P. R. China

Supporting Information

ABSTRACT: Engineered asymmetric membranes for intelligent molecular and ionic transport control at the nanoscale have gained significant attention and offer prospects for broad application in nanofluidics, energy conversion, and biosensors. Therefore, it is desirable to construct a high-performance heterogeneous membrane capable of coordinating highly selective and rectified ionic transport with a simple, versatile, engineered method to mimic the delicate functionality of biological channels. Here, we demonstrate an engineered asymmetric heterogeneous membrane by combining a porous block copolymer (BCP) membrane, polystyrene-*b*-poly(4-vinylpyridine) (PS_{48400}-*b*-$P4VP_{21300}$), with a track-etched asymmetric porous polyethylene terephthalate membrane. The introduction of chemical, geometrical, and electrostatic heterostructures provides our heterogeneous membrane with excellent anion selectivity and ultrahigh ionic rectification with a ratio of ca. 1075, which is considerably higher than that of existing ionic rectifying systems. This anion-selective heterogeneous membrane was further developed into an energy conversion device to harvest the energy stored in an electrochemical concentration gradient. The concentration polarization phenomenon that commonly exists in traditional reverse electrodialysis can be eliminated with an asymmetric bipolar structure, which considerably increases the output power density. This work presents an important paradigm for the use of versatile BCPs in nanofluidic systems and opens new and promising routes to various breakthroughs in the fields of chemistry, materials science, bioscience, and nanotechnology.

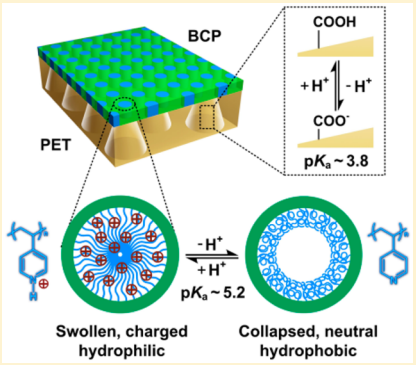

INTRODUCTION

Living organisms make extensive use of nanosized asymmetric ion channels as highly selective filters and ionic rectifiers to control the movement of various ions that play critical roles in life processes, including mass delivery, energy conversion, and signal transmission.[1−4] However, it is difficult to integrate these lipid-membrane-based nanochannels into devices because they are fragile and susceptible to deterioration in changing external environments such as pH, temperature, mechanical stress, etc.[5] The efficiency of these nanochannels in coordinating ionic transport in a highly directional and selective way has been a source of inspiration for scientists seeking to mimic such processes using synthetic asymmetric nanochannel membranes. These synthetic membranes are expected to exhibit similar or stronger functionality compared to their biological counterparts, with superior stability and robustness.[6]

To date, many ingenious asymmetric membranes with homogeneous materials have been developed using various functionalization protocols, such as solution chemical modification, plasma grafting, and ion sputtering technology.[7−10] These challenging nanoscale functionalization processes seriously constrain device performance and future applications,[11,12] which has motivated emerging research of heterogeneous membranes (i.e., hybrid membranes composed of two chemical compositions).[13] Heterogeneous membranes with inherent functional groups are superior because they do not require artificial functionalization. Additionally, compared with homogeneous membranes, heterogeneous membranes are particularly attractive because they can be endowed with novel functionality not available when using two homogeneous membranes separately.[14] For example, Wang et al. demonstrated a multifunctional nanowire-based inorganic heterogeneous membrane that can provide multifunctionality as a single membrane.[15] Our group recently developed an inorganics-based heterogeneous membrane that provides ionic rectifica-

Received: September 21, 2015
Published: November 4, 2015

DOI: 10.1021/jacs.5b09918
J. Am. Chem. Soc. 2015, 137, 14765−14772

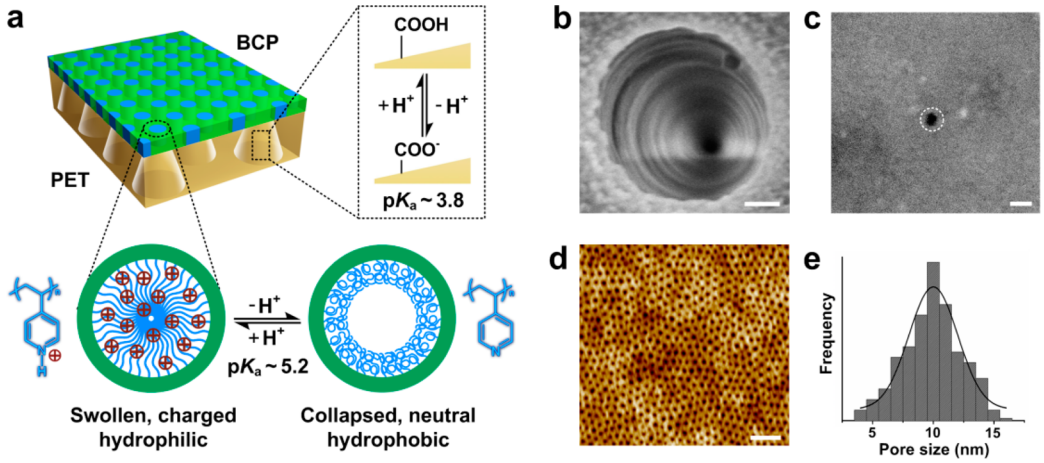

Figure 1. Engineered asymmetric heterogeneous membrane. (a) Schematic of the engineered asymmetric heterogeneous membrane composed of a pH-responsive porous BCP membrane (top layer) and a pH-responsive porous PET membrane with conical nanochannels (bottom layer). (b, c) SEM images of the base (b) and the tip (c) of the conical nanochannels (pore density: 10^7 cm^{-2}). (d) AFM image of the as-prepared BCP membrane atop the PET membrane and a histogram of pore size distribution (pore density: 10^{11} cm^{-2}) with Gaussian fit (e). The scale bars are all 100 nm.

tion with a ratio of ca. 450.[16] The reported results have shown that the fabrication process of inorganics-based heterogeneous membranes is complicated and that material selection is constrained.[13,15−19] Therefore, with regard to mimicking the delicate design of biological channels, it would be desirable to construct a high-performance heterogeneous membrane capable of coordinating highly selective and rectified ionic transport with a simple, versatile, engineered method.

Block copolymer (BCP) is a promising candidate for the construction of a heterogeneous membrane.[20−22] One- and two-dimensional nanofluidic channels can be easily obtained by simply tailoring self-assembled morphologies of the BCP membrane, such as its cylindrical and lamellar structure.[23−25] Because of the structural and functional richness of macromolecular building blocks, the material system is highly versatile, engineered, and scalable and provides well-defined pores.[26−30] Additionally, compared with small molecules,[31−33] end-tethered polymer brushes can provide more effective control over ionic transport because they can increase the spatial density of functional groups on the channel walls by extending the two-dimensional distribution of functional groups to three dimensions.[34−38]

In this article, we demonstrate an engineered asymmetric heterogeneous membrane that can coordinate highly selective and rectified ionic transport by directly coating an porous BCP membrane, polystyrene-*b*-poly(4-vinylpyridine) (PS_{48400}-*b*-$P4VP_{21300}$), onto a robust and flexible porous polyethylene terephthalate (PET) substrate with conical nanochannels. The hybrid membrane, which features asymmetric chemical composition, geometry, and surface charge polarity, exhibits ultrahigh ionic rectification with a notably high ratio of ca. 1075 and excellent anion selectivity. We further developed this anion selective bipolar membrane into a concentration-gradient-driven energy harvesting device. The output power density can be considerably increased because the concentration polarization phenomenon that commonly exists in traditional reverse electrodialysis can be eliminated using the asymmetric bipolar structure. Our newly designed membrane offers several distinct advantages: (1) the heterogeneous membrane can be prepared using a rapid and simple hybridization technique; (2) the rectification ratio (∼1075) is impressive—more than twice the highest ratio reported to date; and (3) the design strategy is versatile and engineered. Various BCPs with different predefined functionalities can be used to further enhance the performance of the heterogeneous membrane. Such a system can trigger further experimental and theoretical efforts to construct "smart" heterogeneous membrane systems for sustainable power generation, water purification, and desalination.[39]

RESULTS AND DISCUSSION

To fabricate the asymmetric heterogeneous membrane, a concentrated viscous solution of BCP in dioxane was spin-coated on a porous PET membrane to form a membrane via microphase separation (Figure 1a).[40] The porous PET membrane substrate (12 μm thick) with conical nanochannels was first prepared by the well-developed ion track etching technique (Figure S1). The large opening of the conical nanochannel is termed the base, and the small opening is termed the tip. In all cases, the diameters of the bases and the tips are approximately 500 and 50 nm, respectively (Figure 1b,c). The nanochannel is electrically neutral as a result of the carboxylate groups generated by the etching process when the membrane is exposed to a solution with a pH below the pK_a (∼3.8). If the pH is above the pK_a, the carboxylate groups deprotonate to produce negative charges on the nanochannel walls.[41]

The as-prepared BCP membrane (∼1.5 μm thick) is composed of a 100 nm-thick layer of hexagonally packed pores (Figure 1d, ∼10 nm) atop a disordered network-like layer. A cross-sectional image of the as-prepared BCP membrane and the corresponding formation mechanism is shown in Figure S2. As shown in Figure 1a, the green segments represent porous matrix formed by the major component, PS, and the blue segments represent channels formed by the minor component, P4VP. The conformational changes of P4VP chains on the inner pore walls and the ionization equilibrium of the pyridine groups (pK_a ≈ 5.2) are also thermodynamically controlled by the pH value.[36,37] The P4VP chains exhibit a swollen, positively charged, and hydrophilic state when the pH is below the pK_a and a collapsed, neutral, and hydrophobic state when the pH is above the pK_a.[42] The conformational changes

DOI: 10.1021/jacs.5b09918
J. Am. Chem. Soc. 2015, 137, 14765−14772

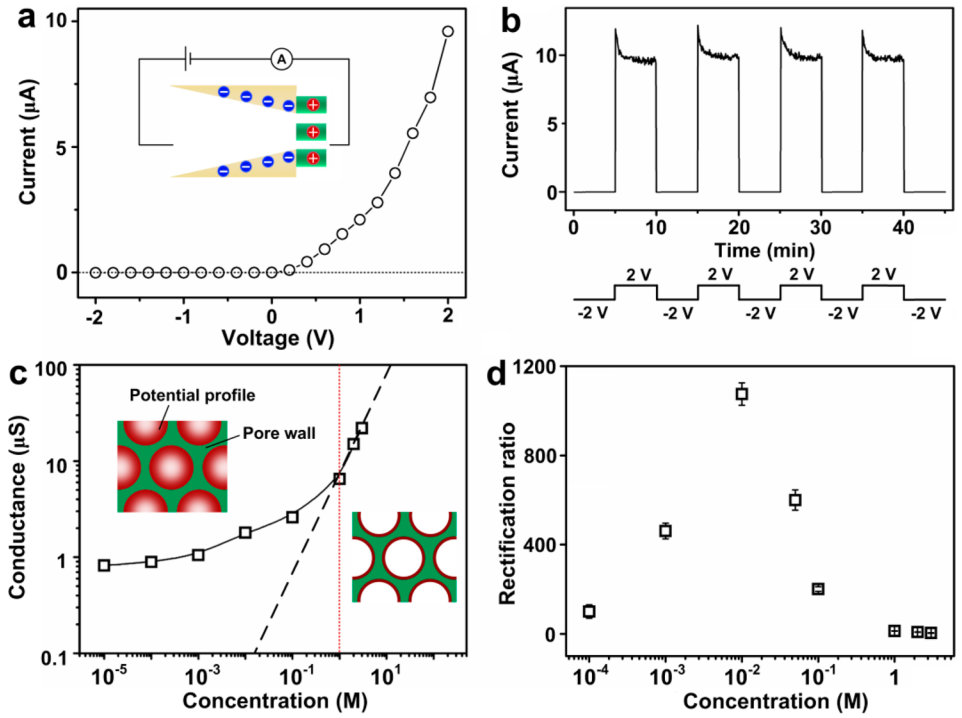

Figure 2. Ultrahigh ionic rectification. (a) $I-V$ curve of the heterogeneous membrane recorded in 10 mM KCl (pH 4.3) when a sweep voltage ranging from −2 to 2 V is applied. The anode is on the PET side, and the cathode is on the BCP side (inset). (b) $I-T$ curve of the heterogeneous membrane recorded in 10 mM KCl (pH 4.3) for an external bias alternating between +2 V/−2 V. (c) Influence of electrolyte concentration on ionic conductance, which displays two distinct regions divided by the red dashed line: a surface charge dominant zone (left) and a bulk concentration dominant zone (right). The transmembrane ionic conductance (black squares) deviates from the bulk value (black dashed line) when the electrolyte concentration is <1 M, indicating a surface charge governed ionic transport. The insets display how the electrical potential profile is altered by electrolyte concentration. (d) Influence of electrolyte concentration on rectifying behavior. The rectification ratio reaches its maximum value of approximately 1075 at intermediate concentration (10 mM); the ratio is sharply reduced at lower and higher KCl concentration regions.

and charged properties of P4VP chains under different pH values are confirmed by Cryo-SEM (Figure S3) and fluorescence characterization (Figure S4), respectively. Through simple hybridization, we get a heterogeneous membrane with chemical, geometrical, and electrostatic heterostructures. In addition, because the solvent evaporates within several seconds during spin coating, the BCP solution with its high viscosity only minimally penetrates into the small PET pores,[43] as confirmed by the SEM image of the interface of the heterogeneous membrane (Figure S5). For simplicity, this minimal penetration is neglected in the following discussion (Figure S9).

The ionic transport properties of the heterogeneous membrane were examined with a simple electrochemical device by measuring the transmembrane ionic current (Figure S6). A pair of Ag/AgCl electrodes was used to apply a transmembrane potential. When placed in a 10 mM KCl electrolyte solution at pH 4.3, the BCP membrane is positively charged, and the PET membrane is negatively charged. They each exhibit slight ionic rectification because of their asymmetric channel geometries.[10,32] Once the heterogeneous membrane is formed, we observed high-performance ionic rectification in the form of an extremely nonlinear current−voltage ($I-V$) curve (Figure 2a). The negative currents are sufficiently small that they are concentric with the x-axis, whereas the positive currents are extremely large. The rectification ratio was as large as 1075 ± 50; such pronounced rectification behavior has not been reported previously.[16,44,45] Figure 2b shows the current−time ($I-T$) curve of the heterogeneous membrane when an external bias of +2 V/−2 V is alternately applied. Both negative and positive currents are relatively constant, indicating the excellent stability of our membrane system.

In general, the ionic rectification originates from broken symmetry, including that of the geometry and surface charge distribution.[46] From the geometry asymmetry, for example, the rectification can be realized in an asymmetric conical PET nanochannel in combination with a homogeneously distributed surface charge.[47] Compared with asymmetric geometry, the asymmetric surface charge distribution (i.e., opposite charge distribution) can achieve higher rectification that cannot be achieved solely by asymmetric geometry. Because for a bipolar nanochannel, the cations and anions are predominantly enriched in the negatively charged side and positively charged side, respectively. Different external bias voltages will cause cations and anions to migrate toward or outward from the junction, resulting in remarkable ion accumulation or depletion in the nanochannel.[48] The ionic rectification can be further strengthened by the two factors synergistically.[49] A typical example is the inorganics-based composite membrane composed of negatively charged mesoporous carbon and positively charged macroporous alumina.[16] In addition to opposite charge distribution, the hybridation of these two symmetric membranes with different pore sizes can provide an incorporated asymmetric geometry that strongly rectifies the ionic current with a ratio of approximately 450; this value is further restricted because of the relatively low degree of geometry asymmetry. Notably, in our case, the existence of a conical PET nanochannel can provide a larger degree of

DOI: 10.1021/jacs.5b09918
J. Am. Chem. Soc. 2015, 137, 14765−14772

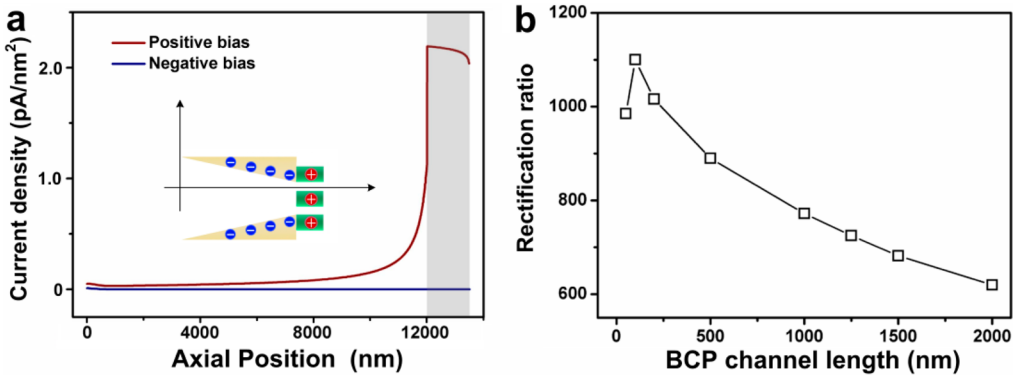

Figure 3. Numerical simulation of ultrahigh ionic rectification. (a) Current density distribution along the axial line of the heterogeneous nanochannel when applying a positive bias of 2 V (red line) and a negative bias of −2 V (blue line). The inset shows the position of the axial line, in which $x = 0$ nm refers to the PET side. The gray zone refers to the BCP nanochannel. (b) Influence of the BCP nanochannel length on the theoretical rectification ratio.

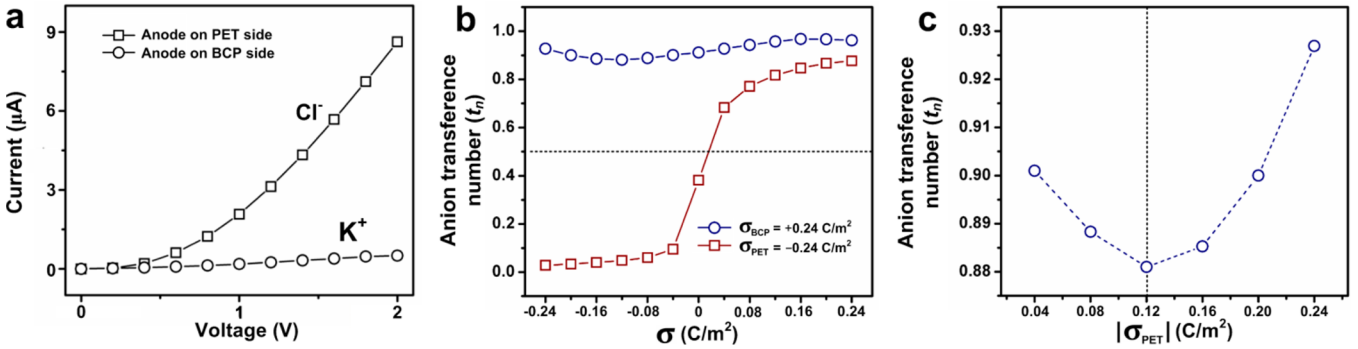

Figure 4. Excellent anion selectivity. (a) $I-V$ curve of the heterogeneous membrane. The membrane is in contact with 0.5 M KCl (pH 4.3) on the BCP side and 10 μM KCl (pH 4.3) on the PET side. Under such a high concentration ratio, the anion selectivity can be verified by the considerably higher Cl^- current compared to the K^+ current. (b, c) Numerical simulation demonstrates excellent anion selectivity. The ion selectivity of the bipolar membrane is dominated by the BCP part because of its smaller pore size (b). Furthermore, the presence of a negatively charged PET channel at the end of the BCP channel promotes anion selectivity across the heterogeneous membrane when the absolute value of charge density in the PET channel is larger than 0.12 C/m^2 (c).

geometry asymmetry, which can accumulate and deplete ions more efficiently and results in a higher rectification of approximately 1075.

The ionic conductance measured in a heterogeneous membrane under the same pH conditions (pH 4.3) is shown in Figure 2c as a function of the electrolyte concentration (KCl). The ionic conductance exhibits a surface charge dominant zone (left) and a bulk concentration dominant zone (right) divided by the red dashed line. The black dashed line represents the bulk behavior of ionic conductance, which is proportional to the ionic concentration. The measured conductance deviates from bulk behavior and exhibits a sharp transition when the electrolyte concentration is less than 1 M. This observation indicates that ionic transport through the heterogeneous membrane is fully governed by the surface charge.[12,50] As the concentration decreases, the electrical potential (red color in insets) generated by the surface charge gradually extends well into the nanochannel as a result of the increasing screening length, which finally results in a more unipolar ionic environment.[51] The electrolyte concentration also has a strong influence on ionic rectification as characterized by the rectification ratio. As shown in Figure 2d, the ratio first increases from 50 to 1075 as the concentration increases from 0.1 to 10 mM. After reaching the maximum value, the ratio decreases to 600 and levels off at approximately 8.0 as the KCl concentration continues to increase (from 10 mM to 3 M). This behavior is in agreement with previous theoretical predications and experimental demonstrations. The ratio is reduced sharply at higher concentrations because of the significantly reduced screening length. In the region of low KCl concentrations, enhanced water dissociation in the bipolar membrane junction under negative bias could be the reason for the reduced ionic rectification.[52,53]

The aforementioned experimental ultrahigh ionic rectification property is quantitatively supported by theoretical simulation based on solving the Poisson and Nernst−Planck (PNP) equations.[54−56] Considering the larger pore size of the thick network layer, in which case the overlapping of double electric layer is much more difficult, ionic transport in the top asymmetric BCP membrane depends strongly on the top thin layer with smaller cylindrical pores.[57] For simplicity, we idealize the nanochannel of the BCP membrane as a straight channel over the entire width of the membrane; additionally, the charges in the polymer brushes are assumed to be strictly confined to the channel walls. This simplification was previously reported by Peinemann et al.[58,59] The simulation model contains a 12 μm-long PET conical nanochannel and a 1500 nm-long cylindrical BCP nanochannel array (Figure S8). The rectifying behavior is illustrated by calculating the current density distribution along the axial line of the heterogeneous channel (Figure 3a). With positive bias, the current density (red line) gradually increases from the base to the tip and undergoes

DOI: 10.1021/jacs.5b09918
J. Am. Chem. Soc. 2015, 137, 14765−14772

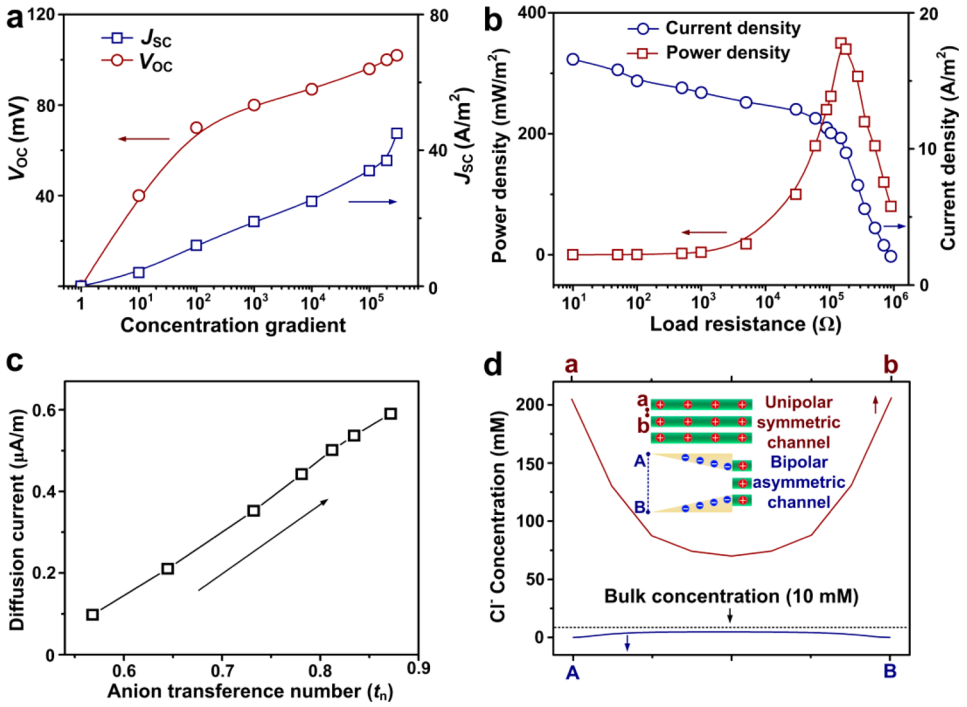

Figure 5. Energy harvesting from a concentration gradient. (a) J_{SC} and V_{OC} recorded under various concentration gradients (KCl). The concentration (KCl) on the PET side remains at 10 μM, and the concentration on the BCP side gradually increases from 10 μM to 3 M. (b) The harvested electrical power can be transferred to an external circuit to supply an external load resistance. For a mixture of 0.5 M NaCl with 0.01 M NaCl, the current density decreases with increasing load resistance, and the corresponding output power density P_L reaches a maximum of approximately 0.35 W/m^2. (c, d) Numerical simulation of high-performance energy harvesting. High anion selectivity is beneficial to the energy harvesting process because it facilitates the generation of net diffusion current (c). Additionally, the asymmetric channel structure and bipolar charge distribution help suppress concentration polarization at the low-concentration side (d). The calculated ion concentration at the orifice of the unipolar symmetric channel (red line) is considerably larger than the bulk value (black dashed line), indicating severe concentration polarization; however, this polarization phenomenon can be eliminated using the bipolar asymmetric channel (blue line).

perturbation across the PET/BCP interface. The current density along the BCP channel is higher than that along the PET channel because the fluid pathway through the BCP channel is narrower than that through the PET channel. In contrast, with negative bias, the current density (blue line) is sufficiently small that it approaches the *x*-axis. This difference in current behavior upon switching the voltage bias is consistent with the experimental data (Figure 2b). The theoretical rectification ratio is approximately 682 (Table S1). The influence of the BCP nanochannel length on the rectifying property is also simulated (Figure 3b). The rectification ratio reaches the maximum value of approximately 1100 with a BCP nanochannel length of 100 nm.[60]

In addition to ultrahigh ionic rectification, the heterogeneous membrane also exhibits excellent anion selectivity. Ion selectivity of the bipolar membrane is probed by ionic current measurements under a concentration gradient.[61] The BCP side is in contact with 0.5 M KCl, and the PET side is in contact with 10 μM KCl, which we believe is sufficiently low to ensure negligible contribution to the measured ionic current. To a good approximation, this method allows us to compare the currents carried by K^+ and Cl^- separately. When the anode is on the PET side, the external bias causes Cl^- to move across the membrane, in which case the Cl^- current is measured (Figure 4a, squares), whereas only a very weak K^+ current is measured if the anode is on the BCP side (Figure 4a, circles). The anion selectivity can be verified by the significantly higher Cl^- current compared to the K^+ current. The symmetric ionic diode with equal pore size, channel length of opposite charge zones, and identical chemical composition is not ion-selective.[62] However, this is totally different from our hybrid system. The introduction of chemical, geometrical, and electrostatic asymmetries not only renders our hybrid membrane ultrahigh ionic rectification but also endows it with excellent anion selectivity.[63]

Because the pore size of BCP part is considerably smaller (and overlapping of the electrical double layers occurs more readily), the overall ion selectivity of the bipolar membrane is dominated by the BCP component. This hypothesis is confirmed by numerical simulation based on PNP theory. If the electrical double layers overlap, the counterion concentration (C) inside the nanochannel is dictated by electroneutrality and depends on the surface charge density: $C \propto \sigma$. This implies that the total ion selectivity can be regulated by varying the surface charge density.[64,65] The overall anion selectivity can be quantified via the calculated anion transference number (t_n).[66,67] If we fix the surface charge density on the BCP side to be 0.24 C/m^2 and vary the surface charge density on the PET side from −0.24 to 0.24 C/m^2, the anion transference number is approximately 0.9 (Figure 4b, blue circles), indicating strong anion selectivity regardless of the charge polarity of the PET side. Notably, the presence of a negatively charged PET channel at the end of the BCP channel augments the selectivity of the device if the absolute value of charge density in the PET channel exceeds 0.12 C/m^2 (Figure 4c). The actual charge density of the PET membrane is larger than this value.[68] The ion selectivity can be reversed by fixing the surface charge density on the PET side to be −0.24 C/m^2

DOI: 10.1021/jacs.5b09918
J. Am. Chem. Soc. 2015, 137, 14765−14772

and varying the surface charge density on the BCP side from −0.24 to 0.24 C/m^2 (Figure 4b, red squares). The calculated anion transference number changes from 0.03 (cation-selective) to 0.87 (anion-selective). Thus, the ion selectivity of the bipolar membrane is dominated by the BCP component because of its smaller pore size. Additionally, if we maintain the surface charge density of the BCP and PET channel at −0.24 and 0.24 C/m^2 and increase the channel size to 20 and 50 nm, the anion transference number is reduced from 0.87 to 0.65 and 0.40, respectively. The increased pore size causes the anion selectivity to decrease to zero. For the nanochannel with a large pore size, the overlapping of electrical double layers is reduced, which consequently causes low ion selectivity.

This anion-selective bipolar membrane was further developed into an energy conversion device to harvest the energy stored in the concentration gradient. Under a concentration gradient, Cl^- diffuses spontaneously across the heterogeneous membrane.[69] Part of the Gibbs free energy inherently available from the concentration gradient can be harvested continuously from the heterogeneous membrane system via the net diffusion current. In the experiment, the heterogeneous membrane was mounted between a two-compartment electrochemical cell. Energy conversion was studied by measuring the scanning $I-V$ cycles in the presence of a concentration gradient across the membrane. All of the electrolyte solutions were adjusted to pH 4.3 to maintain the bipolar charged state. The observed intercept on the current axis (short-circuit current density, J_{SC}) represents the net current flow when no external bias is applied. The intercept on the voltage axis (open-circuit voltage, V_{OC}) represents the diffusion potential, which is contributed by the bipolar power source. Importantly, the contribution from the redox potential on the electrodes can be readily subtracted through the subsequent data analysis (Figure S10).[16,70] The concentration (KCl) on the PET side remains at 10 μM, and the concentration on the BCP side gradually increases from 10 μM to 3 M. The corresponding values of J_{SC} and V_{OC} gradually increase from 0 to 50 A/m^2 and 103 mV, respectively, as the concentration gradient increases from 1 to 3 × 10^5-fold (Figure 5a). Under a reversed salinity gradient from the PET side to the BCP side (e.g., c_{PET}/c_{BCP} = 3 M/10 μM), the inner resistance of the bipolar membrane system increases considerably by approximately 50%, which suppresses energy generation (Figure S11).

The harvested power can also be transferred to an external circuit containing an electrical load resistor. The power consumption of the resistor (R_L) in the circuit can be calculated as $P_L = I_R^2 R_L$. When 0.5 M NaCl is mixed with 0.01 M NaCl, the measured values of V_{OC} and J_{SC} are approximately 80 mV and 20 A/m^2, respectively. The current density (I_R) decreases with increasing load resistance, and P_L reaches its maximum value with an intermediate load resistance (Figure 5b). Similar to the normal voltaic battery, approximately one-fourth of the maximum power ($P_{max} = V_{OC} \times J_{SC}$) can be transferred to the external circuit.[71] The maximum output from the bipolar heterogeneous membrane is as high as 0.35 W/m^2, which exceeds the power efficiency generated by some commercially available cation exchange membranes, including Ionsep, Neosepta, and Qianqiu (Table S6).[72] Regarding the relatively low pore density of the PET membrane (10^7 cm^{-2}), the power density values can be further enhanced using ion-track-etched pores with higher pore density (10^9–10^{10} cm^{-2}). By exploiting parallelization, the predicted power density can reach thousands of watts per square meter, which is comparable to classical reverse electrodialysis with alternative exchange membranes.[73,74]

A numerical simulation is also performed to reveal the underlying mechanism of high-performance energy harvesting. The generation of electrical energy under a concentration gradient originates from the high anion selectivity of the bipolar membrane. The high anion selectivity is beneficial to the energy harvesting process and facilitates the generation of net diffusion current (Figure 5c).[75] Furthermore, in the typical membrane-based reverse electrodialysis process, the practical power output is limited by nonohmic mass-transfer resistances because of the severe concentration polarization occurring at the membrane–solution interface.[76] However, in our reverse electrodialysis process, this polarization phenomenon is rationally eliminated by the physical and chemical design of the nanochannel structure. Under a concentration gradient, the anion (Cl^-) concentration profile at the low concentration side of two types of membrane channels is theoretically compared in Figure 5d. The symmetric unipolar channel exhibits severe concentration polarization (red line), and the anion concentration at the orifice of the low concentration side is considerably higher than the bulk value (dashed line). This implies that the transmembrane Cl^- is enriched at the low-concentration side, which lowers the concentration difference over the membrane and suppresses selective Cl^- transport.[77] This polarization phenomenon disappears when we analyze the asymmetric bipolar channel by simulation because the anion concentration at the channel orifice is lower than the bulk value. In this case, the transmembrane Cl^- is not enriched at the low concentration side because of the negative-charged PET channel, which consequently promotes Cl^- transport.[69,78] Thus, the asymmetric bipolar structure helps to eliminate concentration polarization at the low concentration side, which enables the generation of considerably larger net diffusion currents.

■ CONCLUSIONS

In summary, we demonstrate an engineered heterogeneous membrane with chemical, geometrical, and electrostatic heterostructures by combining a porous BCP membrane and a track-etched asymmetric porous PET membrane. The presence of the PET membrane enables the anion-selective hybrid membrane to exhibit ultrahigh ionic rectification at the remarkably high ratio of ca. 1075 and also promotes overall anion selectivity. We further incorporated the heterogeneous membrane into a concentration-gradient-driven energy harvesting device. Using 0.5 and 0.01 M NaCl solutions, the maximum power output on external electrical load is as high as 0.35 W/m^2, which is notable for a membrane with relatively low pore density. This considerable energy output can be ascribed to the excellent anion selectivity and the elimination of concentration polarization using the asymmetric bipolar structure. This work demonstrates the feasibility of the design strategy of constructing a nanofluidic ion channel membrane system using BCPs. We expect that improved heterogeneous membranes can be fabricated by optimizing the composition and self-assembled morphology of the BCP membrane, thereby opening up applications in sustainable power generation, water purification, and desalination.[79]

■ EXPERIMENTAL SECTION

Materials. Polystyrene-*b*-poly(4-vinylpyridine) (PS_{48400}-*b*-$P4VP_{21300}$ M_w/M_n = 1.13) was purchased from Polymer Source,

DOI: 10.1021/jacs.5b09918
J. Am. Chem. Soc. 2015, 137, 14765–14772

Inc., Canada. Other chemicals were analytical-grade reagents, and all solutions were prepared using degassed Milli-Q water (18.2 MΩ·cm).

Membrane Fabrication. The conical nanochannels (pore density: 10^7 cm^{-2}) were produced in a PET polymer membrane using the well-developed ion track etching technique (Figure S1). To fabricate the heterogeneous membrane, a viscous solution of BCP in dioxane (7 wt %) was spin-coated on the PET membrane and formed an asymmetric membrane via microphase separation.

Electrical Measurement. The ionic transport property of the heterogeneous membrane was determined, and the subsequent energy conversion test was performed by measuring the ionic current through the heterogeneous membrane. The ionic current was measured by a Keithley 6487 picoammeter (Keithley Instruments, Cleveland, OH). The heterogeneous membrane was mounted within a two-compartment electrochemical cell (Figure S6). Ag/AgCl electrodes were used to apply a transmembrane potential.

Numerical Simulation. The steady-state distributions of the ionic current density under external bias were calculated by solving the two-dimensional Poisson and Nernst−Planck (PNP) equations using the commercial finite-element package COMSOL Multiphysics (version 4.4). The "Electrostatics (AC/DC Module)" and "Nernst−Planck without Electroneutrality" modules were used to perform the calculations. The simulated system contained a heterogeneous channel connected by two electrolyte reservoirs. The heterogeneous channel contained a 12 μm-long conically shaped PET channel connected by a cylindrical BCP nanochannel array. Here, we idealized the nanochannel of the BCP membrane as a straight nanochannel system in which the charges of polymer brushes were strictly confined to the channel walls (Figure S8).

■ ASSOCIATED CONTENT

Supporting Information

The Supporting Information is available free of charge on the ACS Publications website at DOI: 10.1021/jacs.5b09918.

Experimental procedures and additional figures (PDF)

■ AUTHOR INFORMATION

Corresponding Author

*wlp@iccas.ac.cn; wen@mail.ipc.ac.cn

Notes

The authors declare no competing financial interest.

■ ACKNOWLEDGMENTS

This work was supported by the National Research Fund for Fundamental Key Projects (2011CB935703, 2011CB935702) National Natural Science Foundation (21171171, 21434003, 91427303, 21201170, 91127025, 21421061), and the Key Research Program of the Chinese Academy of Sciences (KJZD-EW-M03).

■ REFERENCES

(1) Doyle, D. A.; Cabral, J. M.; Pfuetzner, R. A.; Kuo, A.; Gulbis, J. M.; Cohen, S. L.; Chait, B. T.; MacKinnon, R. *Science* **1998**, *280*, 69.
(2) Gouaux, E.; Mackinnon, R. *Science* **2005**, *310*, 1461.
(3) White, R. J.; Ervin, E. N.; Yang, T.; Chen, X.; Daniel, S.; Cremer, P. S.; White, H. S. *J. Am. Chem. Soc.* **2007**, *129*, 11766.
(4) Xu, J.; Lavan, D. A. *Nat. Nanotechnol.* **2008**, *3*, 666.
(5) Xia, F.; Guo, W.; Mao, Y.; Hou, X.; Xue, J.; Xia, H.; Wang, L.; Song, Y.; Ji, H.; Ouyang, Q.; Wang, Y.; Jiang, L. *J. Am. Chem. Soc.* **2008**, *130*, 8345.
(6) Han, C.; Hou, X.; Zhang, H.; Guo, W.; Li, H.; Jiang, L. *J. Am. Chem. Soc.* **2011**, *133*, 7644.
(7) Kalman, E. B.; Vlassiouk, I.; Siwy, Z. S. *Adv. Mater.* **2008**, *20*, 293.
(8) Hou, X.; Dong, H.; Zhu, D.; Jiang, L. *Small* **2010**, *6*, 361.
(9) Hou, X.; Yang, F.; Li, L.; Song, Y.; Jiang, L.; Zhu, D. *J. Am. Chem. Soc.* **2010**, *132*, 11736.
(10) Liu, Q.; Xiao, K.; Wen, L. P.; Dong, Y.; Xie, G. H.; Zhang, Z.; Bo, Z. S.; Jiang, L. *ACS Nano* **2014**, *8*, 12292.
(11) Karnik, R.; Castelino, K.; Duan, C.; Majumdar, A. *Nano Lett.* **2006**, *6*, 1735.
(12) Raidongia, K.; Huang, J. *J. Am. Chem. Soc.* **2012**, *134*, 16528.
(13) Wu, S.; Wildhaber, F.; Vazquez-Mena, O.; Bertsch, A.; Brugger, J.; Renaud, P. *Nanoscale* **2012**, *4*, 5718.
(14) Wu, J.; Wang, N.; Wang, L.; Dong, H.; Zhao, Y.; Jiang, L. *Soft Matter* **2012**, *8*, 5996.
(15) Zhang, J.; Yang, Y.; Zhang, Z.; Wang, P.; Wang, X. *Adv. Mater.* **2014**, *26*, 1071.
(16) Gao, J.; Guo, W.; Feng, D.; Wang, H.; Zhao, D.; Jiang, L. *J. Am. Chem. Soc.* **2014**, *136*, 12265.
(17) Wu, S.; Wildhaber, F.; Bertsch, A.; Brugger, J.; Renaud, P. *Appl. Phys. Lett.* **2013**, *102*, 213108.
(18) Zhang, Q.; Hu, Z.; Liu, Z.; Zhai, J.; Jiang, L. *Adv. Funct. Mater.* **2014**, *24*, 424.
(19) Gracheva, M. E.; Melnikov, D. V.; Leburton, J. P. *ACS Nano* **2008**, *2*, 2349.
(20) Albert, J. N. L.; Epps, T. H. *Mater. Today* **2010**, *13*, 25.
(21) Schacher, F. H.; Rupar, P. A.; Manners, I. *Angew. Chem., Int. Ed.* **2012**, *51*, 7898.
(22) Kim, H. C.; Park, S. M.; Hinsberg, W. D. *Chem. Rev.* **2010**, *110*, 146.
(23) Nunes, S. P.; Behzad, A. R.; Hooghan, B.; Sougrat, R.; Karunakaran, M.; Pradeep, N.; Vainio, U.; Peinemann, K. V. *ACS Nano* **2011**, *5*, 3516.
(24) Tang, C.; Wu, W.; Smilgies, D. M.; Matyjaszewski, K.; Kowalewski, T. *J. Am. Chem. Soc.* **2011**, *133*, 11802.
(25) Shi, W.; Hamilton, A. L.; Delaney, K. T.; Fredrickson, G. H.; Kramer, E. J.; Ntaras, C.; Avgeropoulos, A.; Lynd, N. A. *J. Am. Chem. Soc.* **2015**, *137*, 6160.
(26) Sidorenko, A.; Tokarev, I.; Minko, S.; Stamm, M. *J. Am. Chem. Soc.* **2003**, *125*, 12211.
(27) Bang, J.; Kim, S. H.; Drockenmuller, E.; Misner, M. J.; Russell, T. P.; Hawker, C. J. *J. Am. Chem. Soc.* **2006**, *128*, 7622.
(28) Peinemann, K. V.; Abetz, V.; Simon, P. F. *Nat. Mater.* **2007**, *6*, 992.
(29) Wu, D.; Xu, F.; Sun, B.; Fu, R.; He, H.; Matyjaszewski, K. *Chem. Rev.* **2012**, *112*, 3959.
(30) Yu, H.; Iyoda, T.; Ikeda, T. *J. Am. Chem. Soc.* **2006**, *128*, 11010.
(31) Ali, M.; Ramirez, P.; Mafé, S.; Neumann, R.; Ensinger, W. *ACS Nano* **2009**, *3*, 603.
(32) Wen, L.; Liu, Q.; Ma, J.; Tian, Y.; Li, C.; Bo, Z.; Jiang, L. *Adv. Mater.* **2012**, *24*, 6193.
(33) Kumar, B. V.; Rao, K. V.; Sampath, S.; George, S. J.; Eswaramoorthy, M. *Angew. Chem., Int. Ed.* **2014**, *53*, 13073.
(34) Calvo, A.; Yameen, B.; Williams, F.; Soler-Illia, G.; Azzaroni, O. *J. Am. Chem. Soc.* **2009**, *131*, 10866.
(35) Yameen, B.; Ali, M.; Neumann, R.; Ensinger, W.; Knoll, W.; Azzaroni, O. *J. Am. Chem. Soc.* **2009**, *131*, 2070.
(36) Yameen, B.; Ali, M.; Neumann, R.; Ensinger, W.; Knoll, W.; Azzaroni, O. *Nano Lett.* **2009**, *9*, 2788.
(37) Tagliazucchi, M.; Azzaroni, O.; Szleifer, I. *J. Am. Chem. Soc.* **2010**, *132*, 12404.
(38) Jiang, H.; Xu, F. *Chem. Soc. Rev.* **2013**, *42*, 3394.
(39) Crittenden, J. S.; White, H. S. *J. Am. Chem. Soc.* **2010**, *132*, 4503.
(40) Kim, S. H.; Misner, M. J.; Xu, T.; Kimura, M.; Russell, T. P. *Adv. Mater.* **2004**, *16*, 226.
(41) Siwy, Z.; Gu, Y.; Spohr, H.; Baur, H.; Wolf-Reber, A.; Spohr, R.; Apel, P.; Korchev, Y. *Europhys. Lett.* **2002**, *60*, 349.
(42) Lindqvist, J.; Nyström, D.; Östmark, E.; Antoni, P.; Carlmark, A.; Johansson, M.; Hult, A.; Malmström, E. *Biomacromolecules* **2008**, *9*, 2139.
(43) Rosenholm, J. B. *Adv. Colloid Interface Sci.* **2015**, *220*, 8.
(44) Vlassiouk, I.; Siwy, Z. S. *Nano Lett.* **2007**, *7*, 552.
(45) Cheng, L.; Guo, L. J. *ACS Nano* **2009**, *3*, 575.
(46) Guo, W.; Tian, Y.; Jiang, L. *Acc. Chem. Res.* **2013**, *46*, 2834.
(47) Siwy, Z. S. *Adv. Funct. Mater.* **2006**, *16*, 735.

DOI: 10.1021/jacs.5b09918
J. Am. Chem. Soc. 2015, 137, 14765−14772

(48) Cheng, L. J.; Guo, L. J. *Chem. Soc. Rev.* **2010**, *39*, 923.
(49) Siwy, Z. S.; Howorka, S. *Chem. Soc. Rev.* **2010**, *39*, 1115.
(50) Stein, D.; Kruithof, M.; Dekker, C. *Phys. Rev. Lett.* **2004**, *93*, 035901.
(51) Fan, R.; Huh, S.; Yan, R.; Arnold, J.; Yang, P. *Nat. Mater.* **2008**, *7*, 303.
(52) Bassignana, I. C.; Reiss, H. *J. Membr. Sci.* **1983**, *15*, 27.
(53) Karnik, R.; Duan, C.; Castelino, K.; Daiguji, H.; Majumdar, A. *Nano Lett.* **2007**, *7*, 547.
(54) White, H. S.; Bund, A. *Langmuir* **2008**, *24*, 2212.
(55) White, H. S.; Bund, A. *Langmuir* **2008**, *24*, 12062.
(56) Lan, W. J.; Holden, D. A.; White, H. S. *J. Am. Chem. Soc.* **2011**, *133*, 13300.
(57) Yan, R. X.; Liang, W. J.; Fan, R.; Yang, P. D. *Nano Lett.* **2009**, *9*, 3820.
(58) Qiu, X. Y.; Yu, H. Z.; Karunakaran, M.; Pradeep, N.; Nunes, S. P.; Peinemann, K. V. *ACS Nano* **2013**, *7*, 768.
(59) Zhang, H.; Hou, X.; Zeng, L.; Yang, F.; Li, L.; Yan, D.; Tian, Y.; Jiang, L. *J. Am. Chem. Soc.* **2013**, *135*, 16102.
(60) Vlassiouk, I.; Kozel, T. R.; Siwy, Z. S. *J. Am. Chem. Soc.* **2009**, *131*, 8211.
(61) He, Y.; Gillespie, D.; Boda, D.; Vlassiouk, I.; Eisenberg, R. S.; Siwy, Z. S. *J. Am. Chem. Soc.* **2009**, *131*, 5194.
(62) Vlassiouk, I.; Smirnov, S.; Siwy, Z. *ACS Nano* **2008**, *2*, 1589.
(63) Nguyen, G.; Vlassiouk, I.; Siwy, Z. S. *Nanotechnology* **2010**, *21*, 265301.
(64) Daiguji, H.; Oka, Y.; Shirono, K. *Nano Lett.* **2005**, *5*, 2274.
(65) Vlassiouk, I.; Smirnov, S.; Siwy, Z. *Nano Lett.* **2008**, *8*, 1978.
(66) Zambrowicz, E. B.; Colombini, M. *Biophys. J.* **1993**, *65*, 1093.
(67) Cervera, J.; Alcaraz, A.; Schiedt, B.; Neumann, R.; Ramírez, P. *J. Phys. Chem. C* **2007**, *111*, 12265.
(68) Siwy, Z.; Kosińska, I. D.; Fuliński, A.; Martin, C. R. *Phys. Rev. Lett.* **2005**, *94*, 048102.
(69) Sparreboom, W.; van den Berg, A.; Eijkel, J. C. *Nat. Nanotechnol.* **2009**, *4*, 713.
(70) Alcaraz, A.; Nestorovich, E. M.; Aguilella-Arzo, M.; Aguilella, V. M.; Bezrukov, S. M. *Biophys. J.* **2004**, *87*, 943.
(71) Guo, W.; Cao, L.; Xia, J.; Nie, F.-Q.; Ma, W.; Xue, J.; Song, Y.; Zhu, D.; Wang, Y.; Jiang, L. *Adv. Funct. Mater.* **2010**, *20*, 1339.
(72) Veerman, J.; de Jong, R. M.; Saakes, M.; Metz, S. J.; Harmsen, G. J. *J. Membr. Sci.* **2009**, *343*, 7.
(73) Logan, B. E.; Elimelech, M. *Nature* **2012**, *488*, 313.
(74) Siria, A.; Poncharal, P.; Biance, A. L.; Fulcrand, R.; Blase, X.; Purcell, S. T.; Bocquet, L. *Nature* **2013**, *494*, 455.
(75) Kim, D.; Duan, C.; Chen, Y.; Majumdar, A. *Microfluid. Nanofluid.* **2010**, *9*, 1215.
(76) Post, J. W.; Hamelers, H. V. M; Buisman, C. J. N. *Environ. Sci. Technol.* **2008**, *42*, 5785.
(77) Vermaas, D. A.; Saakes, M.; Nijmeijer, K. *J. Membr. Sci.* **2014**, *453*, 312.
(78) Długołęcki, P.; Gambier, A.; Nijmeijer, K.; Wessling, M. *Environ. Sci. Technol.* **2009**, *43*, 6888.
(79) Wen, L.; Jiang, L. *Natl. Sci. Rev.* **2014**, *1*, 144.

DOI: 10.1021/jacs.5b09918
J. Am. Chem. Soc. 2015, 137, 14765−14772